

Emergence of a neutrino flux above 5 PeV and implications for ultrahigh-energy cosmic rays

Marco S. Muzio ^{1*}, Tianlu Yuan ¹ and Lu Lu ¹

¹Department of Physics and Wisconsin IceCube Particle Astrophysics Center, University of Wisconsin, Madison, WI, 53706, USA.

*Corresponding author(s). E-mail(s): muzio@wisc.edu;

Abstract

The rare detections of astrophysical neutrinos with energies above 5 PeV by two neutrino telescopes underscore the existence of a flux at these energies. In addition to over a decade of data taken by the IceCube Neutrino Observatory, the KM3NeT neutrino telescope has recently highlighted their discovery of a possible $\mathcal{O}(100 \text{ PeV})$ neutrino candidate. A connection between the highest-energy astrophysical neutrinos and the highest-energy cosmic rays is expected, and well-established theoretically. Here, for the first time, we simultaneously fit the neutrino data from IceCube and KM3NeT, as well as the ultrahigh-energy cosmic ray spectrum and composition data from the Pierre Auger Observatory (Auger), to test a common-origin hypothesis. We show that a phenomenological model is able to describe the combined data across these three observatories, and, depending on the true energy of the event detected by KM3NeT, suggests an additional cosmic ray source population not yet robustly detected by Auger. Although a measurement of the neutrino flux in this energy regime is at the sensitivity limit of cubic-kilometer-scale neutrino telescopes, next-generation observatories, such as IceCube-Gen2, will have the sensitivity to make a significant detection of this flux.

Keywords: astrophysical neutrinos, cosmogenic neutrinos, ultrahigh-energy cosmic rays

Main

The origin of ultrahigh-energy cosmic rays (UHECRs) remains one of the enduring mysteries in astrophysics, even after more than a century of research. Recent evidence

now suggests that the atomic mass of cosmic rays becomes increasingly heavy at the highest energies, indicating the presence of a mixed composition [1, 2]. This complicates efforts to trace their origins due to deflections of charged particle trajectories in galactic and extragalactic magnetic fields.

Traditional photon-based astronomy also faces limitations in the study of UHE-CRs. High-energy photons can interact with the cosmic microwave background (CMB) through pair production, significantly reducing their mean free path. These interactions prevent them from being traced directly back to their sources, and challenge efforts to identify UHECR origins through conventional observational methods.

In contrast, neutrinos, produced in the decays of more massive subatomic particles, only interact weakly and can travel from their production sites to Earth almost entirely unimpeded. Due to a rapidly decreasing flux as a function of energy, the detection of high-energy astrophysical neutrinos requires gigaton-scale detectors [3]. Neutrino telescopes, therefore, use natural media as targets, and rely on a sparse array of photomultiplier tubes to detect Cherenkov radiation produced by charged particles following neutrino interactions with the medium. Both natural bodies of water and glacial ice have been tested and employed for this function. In particular, the IceCube Neutrino Observatory has been taking data for over a decade at the South Pole [4], while the KM3NeT Astroparticle Research with Cosmics in the Abyss (ARCA) neutrino telescope is under construction in the Mediterranean Sea [5] and the Baikal-GVD neutrino telescope is under construction in Lake Baikal [6]. Both of the latter observatories have been taking data in partial configurations.

Neutrinos beyond 10 PeV require primary particles with sufficient energy to produce them, and motivate a connection to extragalactic CRs. Modern UHECR observatories, the Pierre Auger Observatory (Auger) and the Telescope Array (TA), have robustly measured both the UHECR spectrum up to $\sim 10^{20.3}$ eV and composition up to $\sim 10^{19.8}$ eV [7]. These measurements have revealed several spectral features: a spectral hardening at $\sim 10^{18.7}$ eV (the *ankle*), a spectral break at $\sim 10^{19}$ eV (the *instep*), and the onset of an apparent cutoff at $\sim 10^{19.7}$ eV [8]. Perhaps most importantly, while the exact composition is unclear due to uncertainties in the hadronic models used to interpret air shower data, the observed composition is inconsistent with a pure-proton hypothesis and, rather, supports a mixed composition [2].

Here, we use a comprehensive sample of neutrinos above 5 PeV towards interpreting the global multimessenger dataset, and present a measurement of the astrophysical neutrino flux beyond 5 PeV. We also highlight the possibility of a non-negligible proton component beyond 30 EeV. Specifically, we perform a joint fit of the neutrino data from IceCube & KM3NeT/ARCA* along with the latest UHECR spectrum and X_{\max} distribution data from Auger to a physically motivated model of UHECR sources. We present the results under different scenarios of the true neutrino energy of the KM3NeT/ARCA candidate, and discuss implications for UHECR modeling and next-generation neutrino telescopes. Details on the methodology of the joint fits are given in the [Methods](#).

*Since Baikal-GVD has not detected any events above 5 PeV, and as it is expected to only marginally contribute to the global exposure, at less than a 2% level, it has a negligible impact on this analysis.

The highest-energy events from IceCube and KM3NeT

The astrophysical neutrino flux has been measured by IceCube starting from around 10 TeV and extending up to around 1 PeV [9–11]. Above ~ 5 PeV, however, IceCube has discovered only three events in independent samples built from different selection routines. Recently, the KM3NeT/ARCA detection of a $\mathcal{O}(100$ PeV) neutrino [12, 13] brings the total number of events at these energies to four. While accumulating sufficient statistics to make a precise flux measurement above 5 PeV likely requires larger next-generation detectors [14], the handful of detections thus far can already provide some constraints on the neutrino flux while also informing UHECR models. Up to now, there has not been a combined analysis of the 5 PeV and higher neutrino data.

Table 1 Summary of neutrino dataset livetimes and properties of the four highest-energy neutrino events assumed in the combined fit to Auger. Note that the inferred neutrino energy can have a dependence on the spectrum and flavor. For the IceCube events we chose the most probable values based on available data. For the KM3NeT/ARCA event, which is less well constrained, we chose two values that span a wide range of possible energies based on Ref. [12].

Dataset	Livetime (yrs)	E_ν (PeV)	Flavor	θ_ν (deg)
IceCube NT	11.8	8.7	μ	101
IceCube HESE	11.8	13.0	μ	68
IceCube PEPE	4.6	6.3	e	74
KM3NeT	1.2	100, 1000	μ	89

Table 1 lists the KM3NeT/ARCA event along with three IceCube events with inferred neutrino energies above 5 PeV. The “Dataset” column indicates the corresponding sample in which the events were discovered. For IceCube, these correspond to three independent selections: the northern track (NT) sample [11, 15], the high-energy starting events (HESE) sample [9, 16, 17], and the PeV partially-contained events (PEPE) sample [18]. Using different techniques, each approach succeeds in isolating a neutrino signal from the substantial down-going atmospheric muon background. The NT sample focuses on selecting muon-induced tracks from the northern sky, primarily from charged current muon neutrino interactions outside the IceCube instrumented volume. The HESE sample targets all-flavor neutrino interactions within a fiducial region of the detector, requiring over 6000 photoelectrons on the PMTs. The PEPE sample is specifically tuned for sensitivity to Glashow resonance [19] detection and expands the effective volume by selecting for electron- and tau-neutrino interactions, as well as muon-neutrino neutral current interactions, occurring near or outside the instrumented region. There is negligible overlap among the three IceCube samples due to their differing signal topology requirements [20]. We assume the latest

livetimes of the three samples. For each event, the most-probable neutrino energy, flavor and zenith angle[†] is taken. While this ignores reconstruction resolutions, such an approximation is reasonable given the large energy and zenith bins used in the binned likelihood construction (c.f. [Methods](#)).

The KM3NeT/ARCA event is possibly the highest-energy neutrino ever detected [[13](#), [21](#)]. ARCA has operated in a partially constructed configuration of 6, 8, 19 and 21 detection units (DU), with their highest-energy event detected under the 21 DU configuration. For this analysis, we approximate the relevant livetime to be roughly that of the combined ARCA19-21 data-taking periods, or about 1.2 years [[22](#)]. Assuming an E^{-2} spectrum, the neutrino energy of the event is estimated to be 220_{-110}^{+570} PeV [[13](#)]. As the uncertainties are large and the energy estimate depends on the spectrum and flavor, we test two different neutrino energy hypotheses: 100 PeV and 1 EeV.

To perform a maximum likelihood analysis, we use the published IceCube effective areas for each sample. Due to instrumentation effects and neutrino Earth absorption, the effective areas are dependent on $(E_\nu, \theta_\nu, \text{flavor})$ as well as the event selection itself. A product of flux, livetime and effective area gives the number of expected astrophysical neutrinos of a given flavor in each sample at a corresponding energy and zenith angle. We approximate the ARCA21 effective area based on its size relative to IceCube, and, given the event morphology, calculate it as roughly 20% of the NT effective area. When multiplied with the livetime this corresponds to 2% of the IceCube NT exposure. Since the samples are independent, a simple sum over their individual log-likelihoods assuming Poisson statistics can be performed. Finally, we assume that backgrounds are negligible above 5 PeV, with atmospheric muons rejected by some combination of overburden or veto [[9](#), [11](#)], and atmospheric neutrino rates suppressed by accompanying muons [[9](#), [23](#)] and model expectations [[11](#), [24](#)].

Ultrahigh-energy cosmic rays and the Pierre Auger Observatory

The flux of UHECRs is extremely low, on the order of ~ 1 per km^2 per century at the highest energies ($\sim 10^{20}$ eV). Detecting them requires observatories with effective collection areas of several thousands of square kilometers. Direct cosmic-ray detectors in space, such as AMS-02, are limited by their small collection areas (a few square meters) and cannot effectively detect UHECRs, despite their ability to measure the charge and mass of lower-energy cosmic rays. Instead, UHECRs can only be detected indirectly through the extensive air showers they initiate in Earth's atmosphere [[24](#)]. These particle showers are observed on the basis of secondary particles arriving at ground-based water Cherenkov detectors, as well as through fluorescent emission in the atmosphere as the shower develops. Modern UHECR observatories leverage both of these observables by combining data from fluorescence telescopes and a ground based array of water Cherenkov tanks. The energy of the primary particle can be robustly estimated from these observables using well-known techniques [[25](#)]. However,

[†]The zenith angle corresponds to the polar angle of the neutrino arrival direction as defined in local detector coordinates; $\theta_\nu = 0$ corresponds to a neutrino entering from directly above the detector.

the primary particle’s chemical composition must be inferred from the energy and depth of shower maximum, X_{\max} , and requires modeling hadronic interactions at ultrahigh energies. While this cannot be done on an event-by-event basis, analysis of the distribution of X_{\max} values at a given energy allows the relative abundances of different nuclei to be inferred. Typically, the first two moments of these distributions are used as input to fit the composition of the UHECR observations. In this work, we instead fit the full X_{\max} distributions in order to take advantage of the additional information encoded in higher-order moments.

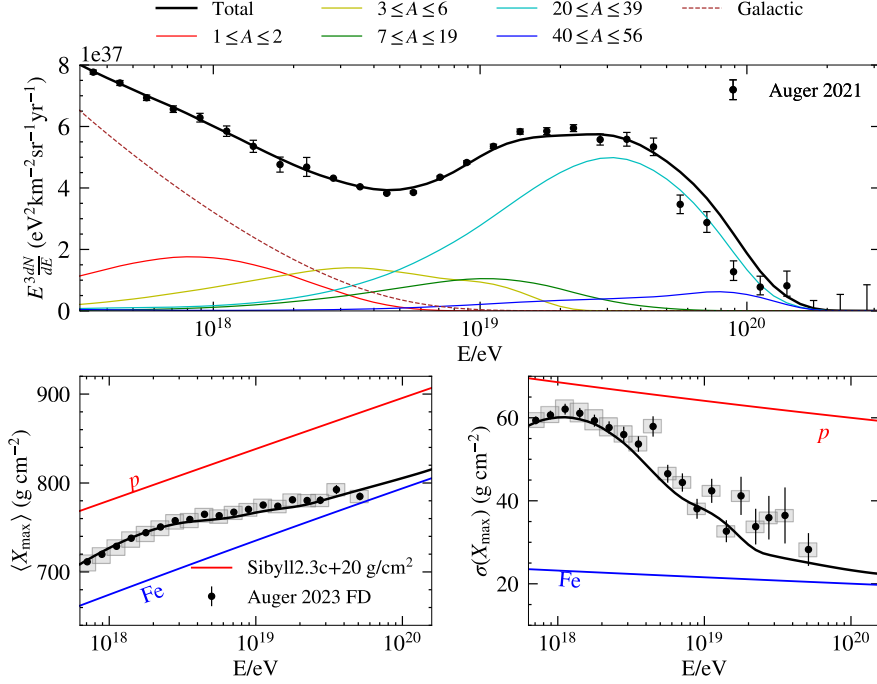


Fig. 1 The measured and predicted CR spectrum (top panel) and X_{\max} moments (bottom panels) for the best-fit model assuming a 100 PeV KM3NeT/ARCA event in the joint likelihood. The total spectrum (black line) is plotted along with the contribution from each mass group and Galactic CRs (colored lines), as compared to observations from Auger [25]. Unfolded $\langle X_{\max} \rangle$ and $\sigma(X_{\max})$ measurements from Auger [1] are plotted along with model predictions interpreted using the SIBYLL2.3c hadronic interaction model (shifted by +20 g/cm^2) and its expectation for pure proton (red line) and Fe (blue line) compositions.

In this work we include two Auger datasets in our joint likelihood. The first is the latest measurement of the CR spectrum above 10^{17} eV [25]. This unfolded spectrum combines 15 years of air shower observations from Auger’s two water Cherenkov detector arrays: the 750 m array and the 1500 m array, encompassing roughly 24 km^2 and 3000 km^2 , respectively.

In addition, we fit the CR composition via the latest published X_{\max} distributions, which have not been corrected for detector effects, including the detector acceptance

and resolution, which can broaden and bias these distributions [1]. This dataset combines roughly 17 years of data from Auger’s 24 fluorescence telescopes, along with observations from three specialized fluorescence telescopes for high-elevation measurements. For visualization purposes, we present the results produced from this dataset as unfolded $\langle X_{\max} \rangle$ and $\sigma(X_{\max})$ measurements. We note that Auger has also recently published $\sigma(X_{\max})$ measurements from surface detector data using a DNN [26, 27], which indicate a narrower X_{\max} distribution above $10^{18.5}$ eV than the fluorescence detector measurements presented here. This data would provide additional constraints on, in particular, the high-energy proton component we explore below. However, given that this data infers an unphysical composition under SIBYLL2.3D (see Figs. 16 and 17 of [27]), we omit it from this work.

Figure 1 shows this latest CR spectrum and composition data from Auger, along with model predictions for the 100 PeV scenario. The spectrum prediction (top panel) is broken down into five mass groups (representing p -, He-, CNO-, Si-, and Fe-like nuclei), as well as, the contribution from Galactic CRs. Air shower observations (bottom panels), in the form of the first two moments of the X_{\max} distribution, are shown relative to expectations for pure proton and Fe compositions, interpreted using SIBYLL2.3C shifted by $+20$ g/cm² based on Ref. [28].

Diffuse joint fit with UHECR and neutrinos

At UHEs, the energy of neutrinos produced by CRs interacting in extragalactic propagation (cosmogenic neutrinos) or inside their source environments (astrophysical neutrinos) is strongly correlated to the energy of the primary CR. In particular, the primary CR’s energy-per-nucleon sets the energy scale of the secondary neutrino, since interactions occur off of individual nucleons due to the much larger center-of-mass energy relative to the nuclear binding energy. The energy of a photohadronically produced neutrino is roughly $E_\nu \simeq E_A/A/20$ [7]. Neutrinos produced hadronically typically have much lower energies than those produced photohadronically, due to the much larger particle multiplicity involved.

Nuclei interactions can also generate neutrinos via photopion production. However, as the photonuclear cross-section at UHEs is dominated by the giant dipole resonance, CR nuclei are more likely to photodisintegrate, a process that results in secondary nucleons, rather than neutrinos, with approximately the same energy-per-nucleon as the parent CR [7, 29]. Given sufficient propagation times, these secondary nucleons can still photopion produce neutrinos with energies comparable to those which their parent nuclei would have created. This process is particularly important for secondary nucleons produced inside source environments, where interaction times are relatively short.

The energy scale of ambient photons sets the threshold energy for CRs to photopion produce. For a target photon with energy ω , this threshold energy is given by $E_A/A = \frac{m_\pi(2m_p+m_\pi)}{4\omega} \simeq 10^{19.5} \left(\frac{\omega}{10^{-3} \text{ eV}}\right)^{-1}$ eV [7]. Since the CR spectrum falls off rapidly, secondary neutrinos will be primarily produced by CRs at threshold. A consequence of this is that neutrinos produced via CR interactions during extragalactic propagation will result in several typical energy scales. Interactions with the CMB result in a peak

neutrino flux at roughly 1 EeV, but require primary CRs with $E_A/A \gtrsim 10^{19.3}$ eV. Interactions with the extragalactic background light (EBL), in particular the cosmic infrared background (CIB), result in a peak neutrino flux at roughly 30 PeV and only require primary CRs with $E_A/A \gtrsim 10^{18}$ eV. Finally, the peak energy of neutrinos produced within source environments will correspond to roughly the lowest energy where there are significant numbers of interactions before escape.

Existing CR spectrum and composition data require only a CR population with sufficient energies to photopion produce with the EBL, but do not rule out a second CR population capable of photopion production off the CMB. Indeed, the long tails of the latest X_{\max} distributions from Auger [1] may hint at a proton contribution at the highest energies [30]. These protons could originate from an additional extragalactic source population that only contributes to the observed UHECR flux at the highest energies, and therefore is not captured by the model explored in [31]. Protons at these energies would be strongly attenuated by interactions with the CMB, a phenomenon referred to as the Greisen-Zatsepin-Kuzmin (GZK) effect [32, 33]. Several recent studies have explored the compatibility of such a pure-proton component at the highest energies with data and its multimessenger implications [34–38]. Notably, these studies have found that a proton component above 10 EeV could make up as much as 10% of the UHECR flux above 50 EeV, while improving fits to the UHECR spectrum & composition data, and saturating current bounds on the neutrino flux above 10 PeV.

The UHECR source model used in this analysis [35, 39, 40] properly accounts for each of these neutrino production processes, as well as Bethe-Heitler energy losses and secondary CR production from photodisintegration inside source environments and in extragalactic propagation. Therefore this model generically predicts both astrophysical and cosmogenic contributions to the neutrino flux. A thorough discussion of the details of this model can be found in the [Methods](#).

Table 2 UHECR-neutrino deviances for the UHECR and SPL models under the two KM3NeT/ARCA energy scenarios. For each combination, the number of degrees of freedom N_{dof} and the total joint deviance D are reported, along with the contributions from the UHECR spectrum $D_{\text{CR},J}$, UHECR composition $D_{\text{CR},X}$, low-energy neutrino data $D_{\nu,\text{lo}}$, and high-energy neutrino data $D_{\nu,\text{hi}}$.

KM3NeT Energy	Model	N_{dof}	D	$D_{\text{CR},J}$	$D_{\text{CR},X}$	$D_{\nu,\text{lo}}$	$D_{\nu,\text{hi}}$
100 PeV	UHECR model	1689	2354.1	1143.4	1156.1	18.2	36.4
100 PeV	SPL model	917	56.7	N/A	N/A	18.1	38.6
1 EeV	UHECR model	1686	1939.4	809.6	1071.8	17.9	40.1
1 EeV	SPL model	917	63.4	N/A	N/A	18.1	45.3

In this section, we analyze the UHECR–neutrino connection using data from Auger, IceCube, and KM3NeT/ARCA. Given the energy uncertainties for the neutrino candidate observed by ARCA21, which is strongly dependent on the underlying neutrino spectrum and flavor, we consider a low- and high-energy scenario. For both cases, we generally assume the arrival flux at Earth follows a 1 : 1 : 1 flavor ratio. The exception is the neutrino flux predicted by the UHECR model, which produces a flavor ratio at Earth that can slightly differ from 1 : 1 : 1. Depending on the model, we

fit to the data by minimizing the joint deviance $D = D_{\text{CR},J} + D_{\text{CR},X} + D_{\nu,\text{lo}} + D_{\nu,\text{hi}}$ to the UHECR and neutrino data, or $D = D_{\nu,\text{lo}} + D_{\nu,\text{hi}}$ to the neutrino data alone (see Table 2). A detailed description of each contribution can be found in the [Methods](#). We find that in the 100 PeV scenario, the observed neutrino data is consistent with a single power-law (SPL) flux, whereas the preferred UHECR model predicts a neutrino component peaking at ~ 30 PeV. In the 1 EeV scenario, we introduce an additional pure proton population at the GZK limit to explore the possibility of the first observed GZK neutrino.

100 PeV case: Implications for the astrophysical neutrino flux

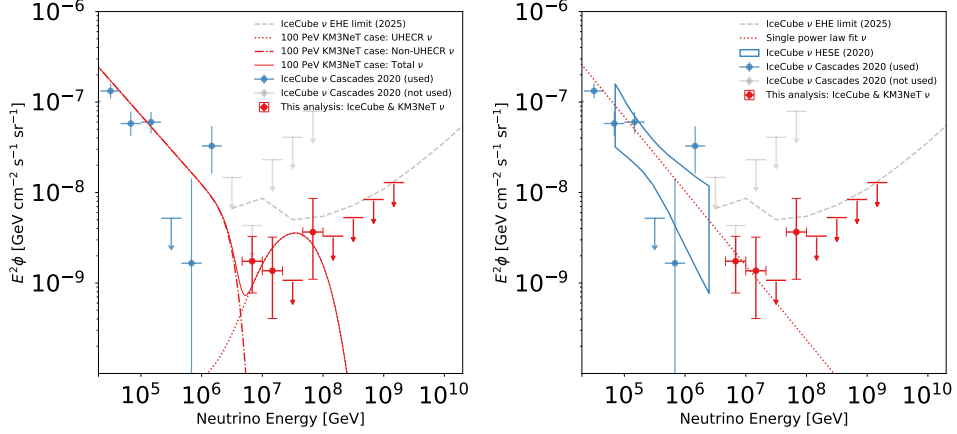


Fig. 2 Results obtained for a 100 PeV KM3NeT/ARCA neutrino. The left panel shows the predicted neutrino flux for the model that best describes the combined neutrino and cosmic ray data. The right panel shows the best-fit single-power law (SPL) flux obtained by fitting the neutrino data alone. The IceCube measured flux from Ref. [10] is shown in solid blue and gray, with the lower energy values (blue) included in the fits. Differential upper limits (90% CL) from Ref. [41] are shown as the dashed gray line. A model independent flux obtained by fitting independent normalization parameters on piecewise segments of an E^{-2} spectrum to the high-energy neutrino data is shown in red.

As a baseline scenario, we assume that the true energy of the neutrino observed by ARCA21 is 100 PeV, consistent with a probable energy estimate in Ref. [21]. Under this assumption we consider two models: an unconstrained, single-power law (SPL) flux and a neutrino flux produced by UHECRs. The results are shown as red lines in Fig. 2. In both cases, the data from Table 1 and the IceCube measured neutrino flux from ~ 30 TeV to ~ 5 PeV (blue) [10] are included in the fit. In the case of the UHECR model (left panel), Auger data is additionally included. The gray upper limits are also from Ref. [10] but are excluded from the model fits in lieu of Table 1.

For comparison, the red error bars show a model independent flux that is obtained by fitting normalization parameters on piecewise segments of an E^{-2} spectrum to the neutrino data in Table 1. Each decade in neutrino energy is broken up into three, equal-log-width segments and the flux normalization within each segment is constrained by constructing a Poisson likelihood based on the expected and observed event counts

when binned over $(E_\nu, \theta_\nu, \text{flavor})$ space. The uncertainties for an individual segment are evaluated using the profile likelihood approach, treating the normalization parameters of other segments as nuisance parameters. In this context, we see the emergence of a neutrino flux at energies beyond 5 PeV.

As the right panel of Fig. 2 shows, a 100 PeV neutrino provides hints of a deviation from the SPL expectation. In contrast, as shown in the left panel, under the assumption that the neutrino flux above 10 PeV is primarily of UHECR-origin, a very different qualitative picture emerges: the SPL spectrum observed at low energies transitions to a UHECR-produced neutrino component with a recovery in the spectrum that peaks around 30 PeV. Although the UHECR-origin model better describes the high-energy neutrino data, as shown in $D_{\nu, \text{hi}}$ in Table 2, at this time there is insufficient statistics to distinguish between these two models above 5 PeV. However, the UHECR prediction can describe both the global neutrino data and the UHECR spectrum and composition data (see Fig. 1), lending it significant phenomenological evidence. We note that while we only present our best-fit model here, many UHECR theoretical and phenomenological models in the literature predict a significantly larger flux above 5 PeV than the SPL model, and refer the reader to Ref. [42] for a concise summary of many such models. A number of astrophysical models for specific source types, including tidal disruption events (TDEs) [43, 44] and jetted active galactic nuclei (AGN) [45], also predict neutrino fluxes peaking in this energy range.

1 EeV case: Implications for the cosmogenic neutrino flux

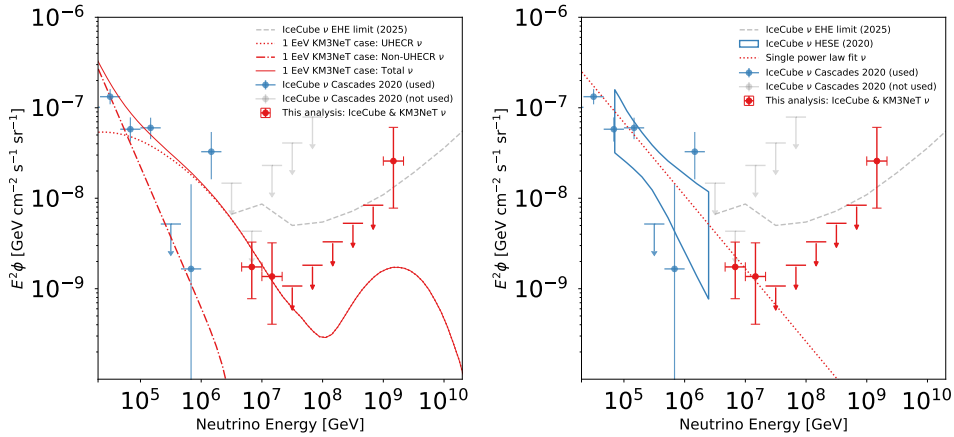


Fig. 3 Same as Fig. 2 except the KM3NeT/ARCA neutrino candidate is assumed have an energy of 1 EeV, and the UHECR model shown in the left panel includes an extra pure-proton population at the highest energies. A 1 EeV neutrino candidate makes it more difficult to reconcile the SPL model shown in the right panel with the neutrino data.

It is also possible that the true neutrino energy is significantly larger than the 100 PeV assumed in the previous section – even as high as 1 EeV. In order to produce such an energetic neutrino, its parent CR would need to have $E_A/A \approx 20$ EeV. The

UHECR model presented in the previous section had a maximum rigidity (energy-per-charge) of less than 10 EeV, in agreement with the results presented in Ref. [31]. For nuclei this translates to a maximum $E_A/A < 5$ EeV. Thus, the baseline UHECR source population assumed earlier is unlikely to produce such an energetic neutrino observation.

A second UHECR source population, driven by a more powerful accelerator, would naturally motivate such an observation. To test this, we include an additional proton component that escapes its source environment with a maximum rigidity above 10 EeV. The compatibility of such a two-component scenario has been investigated by several previous studies using existing UHECR composition data [34–38]. Here, we show that a two-component model could explain a $E_\nu = 1$ EeV KM3NeT/ARCA observation, and explore its implications for UHECR detectors.

Figure 3 shows the predicted neutrino flux for the best-fit two-component UHECR source model (left panel) and the best-fit SPL neutrino flux (right panel) assuming an $E_\nu = 1$ EeV scenario. As in Fig. 2, the red error bars show a model independent measurement of the neutrino flux in piecewise segments of an E^{-2} spectrum, while the blue error bars and gray upper limits are the corresponding measurements from [10]. The predicted neutrino flux produced by the pure-proton component is conservative, in the sense that only cosmogenic interactions are considered for this population. For a comparison of the expected neutrino flux that additionally allows for interactions of protons in the source environment, we refer the reader to [38].

The SPL neutrino spectrum, shown in the right panel of Fig. 3, is only marginally hardened by the KM3NeT/ARCA event, making it more difficult to reconcile this model with the data. However, under the UHECR-origin model, a different picture of the neutrino data emerges as shown in the left panel. The neutrino data up to roughly 10 PeV marks the transition from a low-energy component, which is primarily produced through hadronic interactions of the mixed composition population in their sources, to a UHECR-generated component. In this regime, the data follows to good approximation a SPL, with some deviations from a pure power law visible. Above 100 PeV, a significant recovery in the neutrino spectrum is predicted. These neutrinos are produced via interactions of the pure-proton component with the CMB. Under this model, the KM3NeT/ARCA event would be interpreted as the first observed GZK neutrino, suggesting that a wealth of EeV-scale neutrinos will be observed by the next-generation of neutrino detectors.

A summary of the UHECR spectrum and composition data from Auger and our model predictions is shown in Fig. 4, with the full X_{\max} distributions shown in Fig. 6 in the Methods. The most notable prediction of this model is a recovery of the proton spectrum at Earth above 10 EeV. This results in a deviation of the model’s predicted $\sigma(X_{\max})$ from the Auger published data above roughly 20 EeV [1]. However, due to the relatively low X_{\max} statistics in this energy range, the long-tail of the Gumbel distribution may not yet be adequately characterized to accurately measure $\sigma(X_{\max})$. A more detailed picture of the degree to which our model agrees with current data can be obtained from the full X_{\max} distributions in Fig. 6, which show good agreement

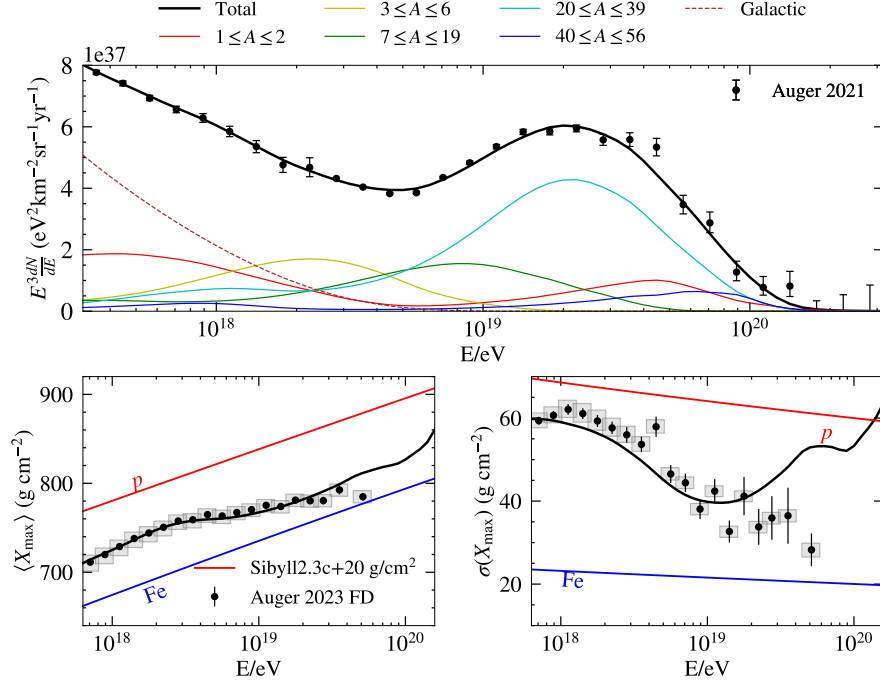


Fig. 4 Same as Fig. 1 for the 1 EeV KM3NeT/ARCA scenario and with an additional proton component at the highest energies. See Fig. 6 for a more detailed comparison of the predicted X_{\max} distributions to data.

between our model and the data. The only significant tension comes from the highest-energy bin, but this is still within uncertainties of the latest proton fractions published by Auger [30].

Conclusion and future prospects

In this work, we explored connections between UHECRs and high-energy neutrinos using data from the world’s largest particle astrophysics observatories—the Pierre Auger Observatory, the IceCube Neutrino Observatory, and the KM3NeT/ARCA neutrino telescope. The results, obtained using the latest publicly available datasets, have implications for models of a common origin of UHECRs and neutrinos.

Our analysis reveals hints of an emerging neutrino population beyond 5 PeV, linked to UHECRs, based on maximum likelihood fits to neutrino and cosmic ray fluxes and cosmic ray X_{\max} distributions. The UHECR-linked neutrinos exhibit a recovery in energy flux, either around 30 PeV or 1 EeV, depending on the assumed neutrino energy of the latest KM3NeT/ARCA candidate. The former is dominated by neutrinos directly produced in UHECR sources, while the latter represents cosmogenic neutrinos from a subset of proton-dominated UHECR sources. Combined with the longer-tailed X_{\max} distributions from Auger, an E_ν of around 1 EeV for the KM3NeT/ARCA

neutrino candidate would be the first indications of an as-yet undiscovered source population of UHE protons.

Of course, the best argument that a significant neutrino flux exists above 5 PeV will be provided by additional neutrino observations at these energies. Based on current estimates, IceCube and KM3NeT/ARCA should be able to detect a handful more events at the lower end of this energy range in the coming years. However, the next-generation of neutrino observatories (with substantially larger observation volumes) will be required in order to distinguish between the SPL expectation and a recovery in the neutrino spectrum.

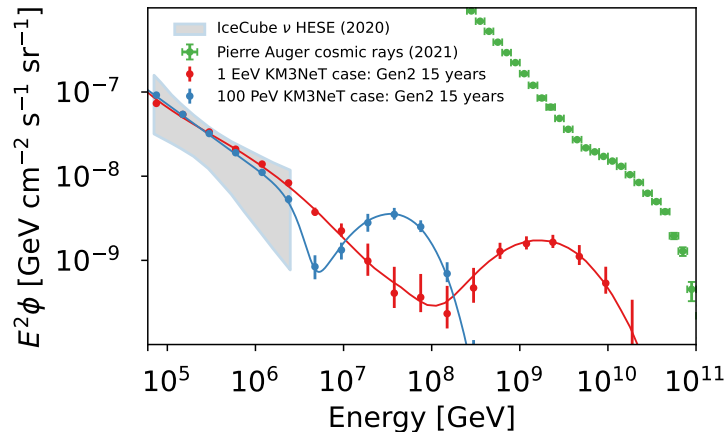


Fig. 5 Projected neutrino flux from an Asimov test for IceCube-Gen2 under the best-fit UHECR- ν models shown in the left panels of Figs. 2 and 3, which respectively correspond to the 100 PeV (blue) and 1 EeV (red) neutrino cases shown here. The shaded region indicates the 1σ uncertainty from a single power-law fit to IceCube’s HESE data [9], and the green curve represents the cosmic-ray flux from the Pierre Auger Observatory [25].

Figure 5 shows the potential for one such observatory, the IceCube-Gen2 detector [46], to discriminate between these possibilities. IceCube-Gen2 has been proposed to expand the instrumented volume of IceCube’s optical array from one to at least eight cubic kilometers. It will feature a core in-ice array of optical sensors, each outfitted with multiple PMTs [47], and a shallow array of radio antennas placed up to ~ 100 m deep in the ice and covering 500 km^2 , significantly enhancing sensitivity to ultrahigh-energy neutrinos at the EeV scale [48]. An Asimov test assuming the common origin model of UHE source neutrinos (blue) and UHE cosmogenic neutrinos (red) is shown in Fig. 5. The sensitivities shown here assumes 15 years of data collection from both the optical and radio components of IceCube-Gen2. The energy and angular resolutions of the Gen2 detector were taken from the Technical Design Report [46], and the fitting tool used was the *toise* software package [49]. If the neutrino flux above 5 PeV is, indeed, dominantly produced by UHECRs (in particular through their interactions in sources), IceCube-Gen2 will have the effective volume required to detect and characterize this flux at a statistically significant level.

The AugerPrime upgrade also offers a valuable opportunity to incorporate ground-based measurements of UHECR mass composition [50], although the primary bottleneck for such joint global-fit analyses remains the limited statistics of neutrino data. After more than a decade of operation, IceCube has detected only three neutrino candidates with energies above 5 PeV. While ARCA eventually will have an effective volume comparable to that of IceCube, significant advancements will require larger target masses and next-generation detectors such as IceCube-Gen2. Future neutrino observatories could provide the necessary data to probe and constrain the properties of UHECR accelerators and their host environments [42], and perhaps allow for joint UHECR-neutrino searches to pinpoint their sources.

Methods

To fit the Auger spectrum and composition measurements, we adopt the Unger-Farrar-Anchordoqui (UFA) CR source model [39] as extended in [35, 40]. Source emission is modeled through a UHECR spectrum injected into a larger environment host to the accelerator. These CRs interact with the environment’s ambient photons and gas (producing secondary nuclei, photons, and neutrinos) while propagating through its turbulent magnetic field. The photodisintegration and spallation interactions in the source generically produce a mixed-composition flux of CRs escaping the source environment. After escaping, UHECRs undergo further photohadronic interactions with the CMB and EBL as they propagate to Earth. Importantly, the UFA model is able to characterize a broad range of source types due to its general source parametrization and lack of absolute scale.

The injected CR spectrum is modeled as a single-power law spectrum with a cut-off predicted by simulations of particle acceleration through magnetically dominated turbulence [51]:

$$J_A(E) \propto E^\gamma \operatorname{sech}[(E/E_{\text{cut},A})^2], \quad (1)$$

where the cutoff energy $E_{\text{cut},A} = Z_A E_{\text{cut},p}$ of each nucleus follows a Peters cycle [52] (composition-independent rigidity cutoff). We approximate the composition of the accelerated spectrum through five nuclei (representing p , He-like, CNO-like, Si-like, and Fe-like mass groups) with relative abundances as free parameters of the model. In total the injected CR spectrum is characterized through 7 free parameters.

The source environment is characterized through 5 free parameters which (indirectly) control the photon-to-gas density, relative magnetic field strength and coherence length, and relative source size. These parameters are discussed in-depth in [40, 53]. Sources are assumed to be standard, modulo their relative luminosity-density which is captured through a model of their cosmological evolution. For simplicity, we assume this evolution follows the star formation rate (SFR) evolution [54] up to a maximum comoving distance of 4.2 Gpc.

A single-power law Galactic CR spectrum (with exponential cutoff) is added to the predicted CR spectrum as a nuisance component to model the Galactic-to-extragalactic transition. For simplicity, we approximate this component as having a pure composition. The Galactic nuisance component adds 4 free parameters.

Extragalactic propagation is modeled using pre-tabulated propagation matrices generated using CRPROPA3 [55] assuming EBL model from [56] and photodisintegration cross-sections from TALYS v1.8 [57].

In the case of the 1 EeV KM3NeT/ARCA event scenario, we consider one additional extragalactic CR component: a pure-proton component with an escaping spectrum parametrized by a single-power law and exponential cutoff. This component is assumed to come from a second source population (given their much larger rigidity cutoff) with few in-source interactions. For simplicity we assume this population also follows a SFR evolution. This second proton component adds 3 additional free parameters to the model.

The neutrino flux is modeled through two components. The first component, which dominates at high energies, is the neutrino flux produced by UHECRs inside sources and through extragalactic propagation. This component is fully captured by the model described above and adds no additional free parameters. The second component, which serves as a nuisance component to capture the low-to-high energy transition, is modeled as a single-power law with a cutoff following the same functional form as that in (1) (with an assumed 1 : 1 : 1 flavor ratio). This low-energy neutrino nuisance component adds 3 free parameters.

In total, the baseline UHECR source model has 19 free parameters. If a second proton component is considered, there are 22 total free parameters. These parameters are fit to maximize the joint likelihood to the UHECR spectrum & composition and neutrino data. In practice, this is carried out by minimizing the deviance $D = -2\ln(L/L_{\text{sat}})$, where L is the model likelihood and L_{sat} is the likelihood of a model that perfectly describes the data. The total deviance used in the minimization of the UHECR model is given by $D = D_{\text{CR},J} + D_{\text{CR},X} + D_{\nu,\text{lo}} + D_{\nu,\text{hi}}^\ddagger$.

The UHECR spectrum is fit using a saturated Poisson likelihood

$$D_{\text{CR},J} = 2 \sum_i m_i - d_i + d_i \ln(d_i/m_i) , \quad (2)$$

where the sum is over energy bins $17.5 \leq \lg(E_i/\text{eV}) \leq 22$, d_i is the observed number of events in bin i , and m_i is the predicted number of events by the model. Spectrum data points are taken from [25].

Following [31], the UHECR composition data (namely, the depth of shower maximum distributions) are fit using a multinomial likelihood

$$D_{\text{CR},X} = 2 \sum_{i,j} d_{ij} \ln \left(\frac{d_{ij}}{n_i p_{ij}} \right) , \quad (3)$$

where the sum is over energy bins $17.8 \leq \lg(E_i/\text{eV}) \leq 20$ and depth of shower maximum bins $500 \text{ g/cm}^2 \leq X_{\text{max},j} \leq 1300 \text{ g/cm}^2$, n_i is the total number of observed events in the i th bin's X_{max} distribution, d_{ij} is the number of observed events in the j th X_{max} bin, and p_{ij} is the model probability for a shower in energy bin i to have X_{max} falling in the j th bin. p_{ij} is given by a sum of probability distributions $G_{\text{reco},ij}^A$

[‡]The SPL and segmented neutrino flux models are constrained by the neutrino data alone.

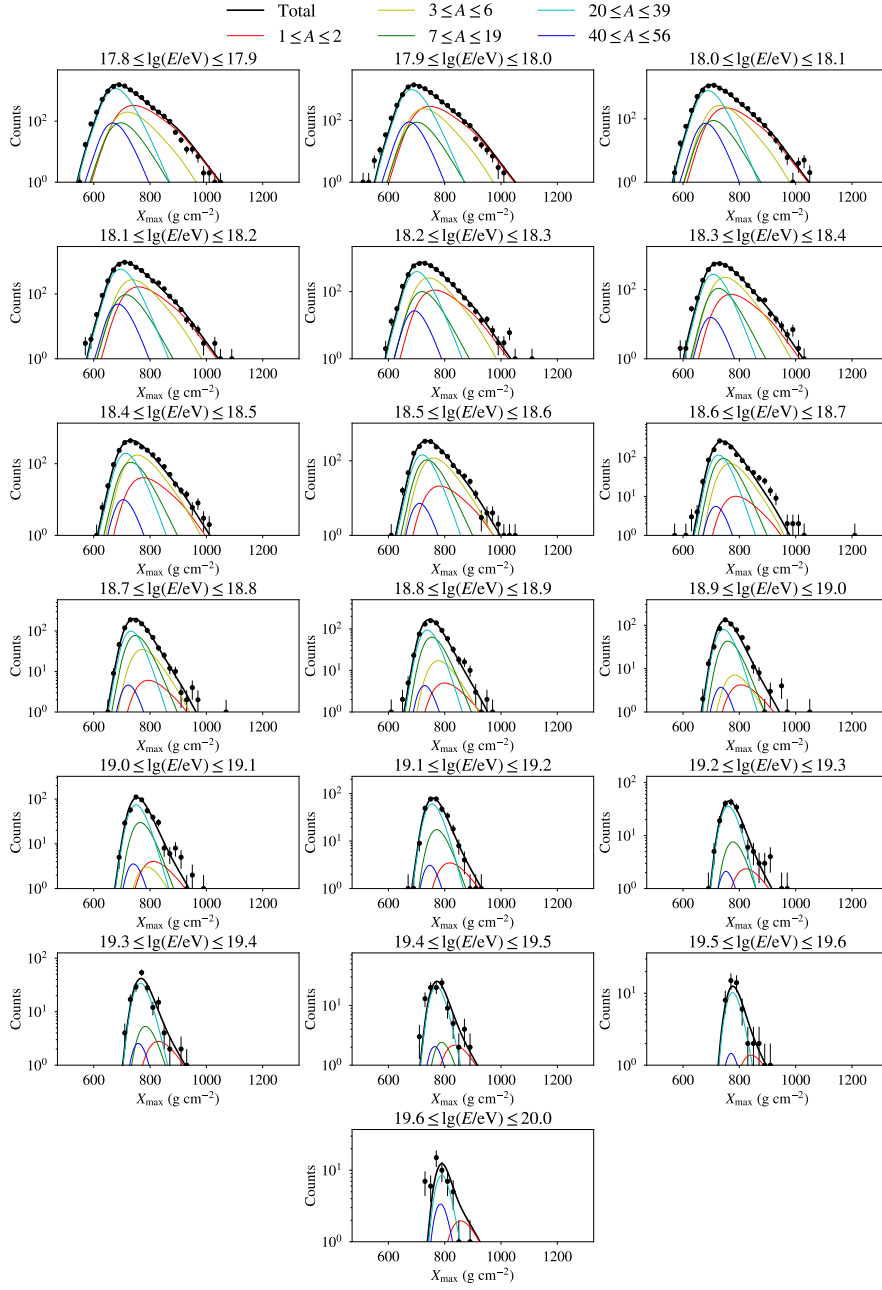


Fig. 6 Predicted X_{\max} distribution for the best-fit model with an additional high energy proton component, assuming a 1 EeV KM3NeT/ARCA event. The total forward-folded distribution (black lines) is compared to Auger measurements [1], and broken down by mass group contribution (colored lines).

weighted by the fraction of the total model flux contributed by CRs of mass A . These probability distributions are calculated by forward folding the generalized Gumbel distribution G_{ij}^A for a CR with mass A and energy E_i with the Auger acceptance and resolution [58]. We use the parameters from [59] for SIBYLL2.3C [60] for the true generalized Gumbel distributions, adding an additional $+20 \text{ g/cm}^2$ to the distribution based on [28]. The X_{max} data points are taken from [1].

The neutrino likelihood is split into a low- and high-energy contribution. At lower energies, where more statistics are available, it becomes important but challenging to model the background, detector and systematic uncertainties. Thus, we fit to the published neutrino flux directly as that includes these effects to the best of our knowledge at the time. We use the best-fit piecewise differential flux as measured by IceCube in Ref. [10], converted to an all-flavor flux assuming a 1:1:1 flavor ratio. The measured flux in each piecewise segment has asymmetric errors (or upper bounds) that contain both statistical and systematic uncertainties. In order to incorporate these measurements into a likelihood, we assume the measured flux in each segment can be modeled by a gamma distribution whose mode is set to the published best-fit point. This is motivated by interpreting the gamma distribution as a continuous analog of the negative binomial distribution, which itself generalizes the Poisson distribution to allow for a variance that differs from the mean and hence can model additional uncertainties on top of pure Poisson statistics. The gamma log-likelihood is then given by

$$D_{\nu,\text{lo}} = 2 \sum_i (\alpha_i - 1) \ln(y_i/\phi_i) + (\phi_i - y_i)/\theta_i, \quad (4)$$

where the sum is over energy bins $30 \text{ TeV} \leq E_i \leq 2 \text{ PeV}$, y_i is the central value of the piecewise flux in that bin, and ϕ_i is the predicted all-flavor flux under our model. The parameters α_i and θ_i correspond to the shape and scale parameters of the underlying gamma distribution, and are fixed by the best-fit point and its associated uncertainty. That is, for a given energy bin i , α_i and θ_i are obtained by solving the following system of equations,

$$\begin{cases} y_i = (\alpha_i - 1)\theta_i \\ \int_{y_i - \sigma_i^-}^{y_i + \sigma_i^+} \text{Gamma}(x; \alpha_i, \theta_i) dx = 0.68, \end{cases} \quad (5)$$

where σ_i^\pm are the upper and lower error bars reported on y_i and $\text{Gamma}(x; \alpha_i, \theta_i)$ is the probability density function of the gamma distribution. In the case of a reported upper limit, we take $y_i = \sigma_i^- = 0$.

At neutrino energies above 5 PeV, where only four neutrino events have been observed by both IceCube and KM3NeT, we again use a saturated Poisson likelihood. The deviance is given by

$$D_{\nu,\text{hi}} = 2 \sum_{E_i < 1 \text{ EeV}} \sum_{a,k,\rho} m_{aik\rho} - d_{aik\rho} + d_{aik\rho} \ln(d_{aik\rho}/m_{aik\rho}) + 2 \sum_{E_i \geq 1 \text{ EeV}} m_i. \quad (6)$$

Below 1 EeV, a indexes the neutrino datasets given in Table 1, ρ the neutrino flavor, i the neutrino energy, k the $\cos \theta_k$ zenith bins, and d and m represent the observed and predicted number of events in a bin, respectively. To calculate $m_{aik\rho}$ the predicted single-flavor flux $\phi_{\nu_\rho+\bar{\nu}_\rho}$ is multiplied by the exposure of dataset a to flavor ρ neutrinos and integrated over the area of the ik th energy- $\cos \theta$ bin. Note that this assumes an isotropic flux. As described in the main text and listed, three IceCube and one KM3NeT/ARCA datasets are included. The effective areas for each of these datasets were extrapolated to 1 EeV where necessary.

Above 1 EeV, the non-observation of neutrinos is modeled by calculating the total number of neutrinos m_i predicted in the i th energy bin when multiplied to the latest IceCube exposure from Ref. [41, 61].

Acknowledgements. We acknowledge the use of code created by Michael Unger under the EU-funded Grant PEOF-GA2013-624803 and further developed by M.M. . We thank Albrecht Karle and Michael Unger for reading through an earlier version of the manuscript and providing valuable comments. M.M. acknowledges support from NSF MPS-Ascend Postdoctoral Award #2138121 and the John Bahcall Fellowship at the Wisconsin IceCube Particle Astrophysics Center at the University of Wisconsin–Madison. T.Y. and L.L are supported in part by NSF grant PHY-2209445 and by the University of Wisconsin Research Committee with funds granted by the Wisconsin Alumni Research Foundation.

References

- [1] Abreu, P. *et al.* Depth of Maximum of Air-Shower Profiles above $10^{17.8}$ eV Measured with the Fluorescence Detector of the Pierre Auger Observatory and Mass Composition Implications. *PoS ICRC2023*, 319 (2023).
- [2] Abdul Halim, A. *et al.* Depth of maximum of air-shower profiles: testing the compatibility of the measurements at the Pierre Auger Observatory and the Telescope Array. *PoS ICRC2023*, 249 (2023).
- [3] Halzen, F., Learned, J. & Stanev, T. Neutrino Astronomy. *AIP Conf. Proc.* **198**, 39–51 (1990).
- [4] Aartsen, M. G. *et al.* The IceCube Neutrino Observatory: Instrumentation and Online Systems. *JINST* **12**, P03012 (2017).
- [5] Aiello, S. *et al.* Astronomy potential of KM3NeT/ARCA. *Eur. Phys. J. C* **84**, 885 (2024).
- [6] Zaborov, D. Neutrino astronomy at Lake Baikal (2024).
- [7] Anchordoqui, L. A. Ultra-High-Energy Cosmic Rays. *Phys. Rept.* **801**, 1–93 (2019).
- [8] Bergman, D. R. *et al.* Measurement of UHECR energy spectrum with the Pierre Auger Observatory and the Telescope Array. *PoS ICRC2023*, 406 (2024).
- [9] Abbasi, R. *et al.* The IceCube high-energy starting event sample: Description and flux characterization with 7.5 years of data. *Phys. Rev. D* **104**, 022002 (2021).
- [10] Aartsen, M. G. *et al.* Characteristics of the diffuse astrophysical electron and tau neutrino flux with six years of IceCube high energy cascade data. *Phys. Rev. Lett.* **125**, 121104 (2020).

- [11] Abbasi, R. *et al.* Improved Characterization of the Astrophysical Muon–neutrino Flux with 9.5 Years of IceCube Data. *Astrophys. J.* **928**, 50 (2022).
- [12] KM3NeT Collaboration. Latest Results from KM3NeT. Presented at the XXXI International Conference on Neutrino Physics and Astrophysics (2024). URL <https://agenda.infn.it/event/37867/>. Conference presentation.
- [13] Aiello, S. *et al.* Observation of an ultra-high-energy cosmic neutrino with KM3NeT. *Nature* **638**, 376–382 (2025). URL <https://doi.org/10.1038/s41586-024-08543-1>.
- [14] Aartsen, M. G. *et al.* IceCube-Gen2: the window to the extreme Universe. *J. Phys. G* **48**, 060501 (2021).
- [15] Naab, R., Ganster, E. & Zhang, Z. Measurement of the astrophysical diffuse neutrino flux in a combined fit of IceCube’s high energy neutrino data. *PoS ICRC2023*, 1064 (2023).
- [16] Aartsen, M. G. *et al.* Evidence for High-Energy Extraterrestrial Neutrinos at the IceCube Detector. *Science* **342**, 1242856 (2013).
- [17] Abbasi, R. *et al.* Updated directions of IceCube HESE events with the latest ice model using DirectFit. *PoS ICRC2023*, 1030 (2023).
- [18] Aartsen, M. G. *et al.* Detection of a particle shower at the Glashow resonance with IceCube. *Nature* **591**, 220–224 (2021). [Erratum: *Nature* 592, E11 (2021)].
- [19] Glashow, S. L. Resonant scattering of antineutrinos. *Phys. Rev.* **118**, 316–317 (1960). URL <https://link.aps.org/doi/10.1103/PhysRev.118.316>.
- [20] Lu, L. Multi-flavour PeV neutrino search with IceCube. *PoS ICRC2017*, 1002 (2018).
- [21] Coelho, J. Latest results from KM3NeT (2024). URL <https://doi.org/10.5281/zenodo.12706075>.
- [22] KM3NeT Collaboration. The search for point-like neutrino sources with antares and km3net/arca telescopes. Presented at the 9th edition of the Roma International Conference on AstroParticle Physics (2024). URL <https://agenda.infn.it/event/35353/>. Conference presentation.
- [23] Argüelles, C. A., Palomares-Ruiz, S., Schneider, A., Wille, L. & Yuan, T. Unified atmospheric neutrino passing fractions for large-scale neutrino telescopes. *JCAP* **07**, 047 (2018).
- [24] Workman, R. L. & Others. Review of Particle Physics. *PTEP* **2022**, 083C01 (2022).
- [25] Abreu, P. *et al.* The energy spectrum of cosmic rays beyond the turn-down around 10^{17} eV as measured with the surface detector of the Pierre Auger Observatory. *Eur. Phys. J. C* **81**, 966 (2021).
- [26] Abdul Halim, A. *et al.* Inference of the Mass Composition of Cosmic Rays with Energies from 1018.5 to 1020 eV Using the Pierre Auger Observatory and Deep Learning. *Phys. Rev. Lett.* **134**, 021001 (2025).
- [27] Abdul Halim, A. *et al.* Measurement of the depth of maximum of air-shower profiles with energies between 1018.5 and 1020 eV using the surface detector of the Pierre Auger Observatory and deep learning. *Phys. Rev. D* **111**, 022003 (2025).

- [28] Abdul Halim, A. *et al.* Testing hadronic-model predictions of depth of maximum of air-shower profiles and ground-particle signals using hybrid data of the Pierre Auger Observatory. *Phys. Rev. D* **109**, 102001 (2024).
- [29] Murase, K. & Beacom, J. F. Neutrino Background Flux from Sources of Ultrahigh-Energy Cosmic-Ray Nuclei. *Phys. Rev. D* **81**, 123001 (2010).
- [30] Abdul Halim, A. *et al.* Studies of the mass composition of cosmic rays and proton-proton interaction cross-sections at ultra-high energies with the Pierre Auger Observatory. *PoS ICRC2023*, 438 (2023).
- [31] Halim, A. A. *et al.* Constraining the sources of ultra-high-energy cosmic rays across and above the ankle with the spectrum and composition data measured at the Pierre Auger Observatory. *JCAP* **05**, 024 (2023).
- [32] Greisen, K. End to the cosmic ray spectrum? *Phys. Rev. Lett.* **16**, 748–750 (1966).
- [33] Zatsepin, G. T. & Kuzmin, V. A. Upper limit of the spectrum of cosmic rays. *JETP Lett.* **4**, 78–80 (1966).
- [34] van Vliet, A., Alves Batista, R. & Hörandel, J. R. Determining the fraction of cosmic-ray protons at ultrahigh energies with cosmogenic neutrinos. *Phys. Rev. D* **100**, 021302 (2019).
- [35] Muzio, M. S., Unger, M. & Farrar, G. R. Progress towards characterizing ultrahigh energy cosmic ray sources. *Phys. Rev. D* **100**, 103008 (2019).
- [36] Anker, A. *et al.* White Paper: ARIANNA-200 high energy neutrino telescope (2020).
- [37] Ehlert, D., van Vliet, A., Oikonomou, F. & Winter, W. Constraints on the proton fraction of cosmic rays at the highest energies and the consequences for cosmogenic neutrinos and photons. *JCAP* **02**, 022 (2024).
- [38] Muzio, M. S., Unger, M. & Wissel, S. Prospects for joint cosmic ray and neutrino constraints on the evolution of trans-Greisen-Zatsepin-Kuzmin proton sources. *Phys. Rev. D* **107**, 103030 (2023).
- [39] Unger, M., Farrar, G. R. & Anchordoqui, L. A. Origin of the ankle in the ultrahigh energy cosmic ray spectrum, and of the extragalactic protons below it. *Phys. Rev. D* **92**, 123001 (2015).
- [40] Muzio, M. S., Farrar, G. R. & Unger, M. Probing the environments surrounding ultrahigh energy cosmic ray accelerators and their implications for astrophysical neutrinos. *Phys. Rev. D* **105**, 023022 (2022).
- [41] Abbasi, R. *et al.* A search for extremely-high-energy neutrinos and first constraints on the ultra-high-energy cosmic-ray proton fraction with IceCube. *arXiv preprint* 2502.01963 (2025).
- [42] Valera, V. B., Bustamante, M. & Glaser, C. Near-future discovery of the diffuse flux of ultrahigh-energy cosmic neutrinos. *Phys. Rev. D* **107**, 043019 (2023).
- [43] Biehl, D., Boncioli, D., Lunardini, C. & Winter, W. Tidally disrupted stars as a possible origin of both cosmic rays and neutrinos at the highest energies. *Sci. Rep.* **8**, 10828 (2018).
- [44] Plotko, P., Winter, W., Lunardini, C. & Yuan, C. Ultra-High-Energy Cosmic Rays from Neutrino-Emitting Tidal Disruption Events (2024).

- [45] Rodrigues, X., Heinze, J., Palladino, A., van Vliet, A. & Winter, W. Active Galactic Nuclei Jets as the Origin of Ultrahigh-Energy Cosmic Rays and Perspectives for the Detection of Astrophysical Source Neutrinos at EeV Energies. *Phys. Rev. Lett.* **126**, 191101 (2021).
- [46] Abbasi, R. *et al.* The IceCube-Gen2 Neutrino Observatory: Technical Design Report, Parts I, II, and III (2024). URL <https://icecube-gen2.wisc.edu/science/publications/tdr/>.
- [47] Makino, Y. *et al.* Mechanical design of the optical modules intended for IceCube-Gen2. *PoS ICRC2023*, 979 (2023).
- [48] Ishihara, A. *et al.* The next generation neutrino telescope: IceCube-Gen2. *PoS ICRC2023*, 994 (2023).
- [49] van Santen, J., Clark, B. A., Halliday, R., Hallmann, S. & Nelles, A. toise: a framework to describe the performance of high-energy neutrino detectors. *JINST* **17**, T08009 (2022).
- [50] Aab, A. *et al.* The Pierre Auger Observatory Upgrade - Preliminary Design Report (2016).
- [51] Comisso, L., Farrar, G. R. & Muzio, M. S. Ultra-High-Energy Cosmic Rays Accelerated by Magnetically Dominated Turbulence. *Astrophys. J. Lett.* **977**, L18 (2024).
- [52] Peters, B. Primary cosmic radiation and extensive air showers. *Nuovo Cim.* **22**, 800–819 (1961).
- [53] Muzio, M. S. & Farrar, G. R. Constraints on the Hosts of UHECR Accelerators. *Astrophys. J. Lett.* **942**, L39 (2023).
- [54] Robertson, B. E., Ellis, R. S., Furlanetto, S. R. & Dunlop, J. S. Cosmic Reionization and Early Star-forming Galaxies: a Joint Analysis of new Constraints From Planck and the Hubble Space Telescope. *Astrophys. J. Lett.* **802**, L19 (2015).
- [55] Alves Batista, R. *et al.* CRPropa 3 - a Public Astrophysical Simulation Framework for Propagating Extraterrestrial Ultra-High Energy Particles. *JCAP* **05**, 038 (2016).
- [56] Gilmore, R. C., Somerville, R. S., Primack, J. R. & Dominguez, A. Semi-analytic modeling of the EBL and consequences for extragalactic gamma-ray spectra. *Mon. Not. Roy. Astron. Soc.* **422**, 3189 (2012).
- [57] Koning, A. J., Hilaire, S. & Duijvestijn, M. C. TALYS: Comprehensive Nuclear Reaction Modeling. *AIP Conf. Proc.* **769**, 1154 (2005).
- [58] Aab, A. *et al.* Depth of Maximum of Air-Shower Profiles at the Pierre Auger Observatory: Measurements at Energies above $10^{17.8}$ eV. *Phys. Rev. D* **90**, 122005 (2014).
- [59] Arbeletche, L. B. & de Souza, V. On the parametrization of the distributions of depth of shower maximum of ultra-high energy extensive air showers. *Astropart. Phys.* **116**, 102389 (2020).
- [60] Fedynitch, A., Riehn, F., Engel, R., Gaisser, T. K. & Stanev, T. Hadronic interaction model sibyll 2.3c and inclusive lepton fluxes. *Phys. Rev. D* **100**, 103018 (2019).
- [61] Data release for A search for extremely-high-energy neutrinos and first constraints on the ultra-high-energy cosmic-ray proton fraction with IceCube (2025). URL

<https://doi.org/10.7910/DVN/JHK49D>.